[Article] www.whxb.pku.edu.cn

乙酸乙酯在 Al_2O_3-$Ce_{0.5}Zr_{0.5}O_2$ 负载的金属氧化物催化剂上的催化燃烧

袁书华 沈 美 龚茂初 王健礼 闫生辉 曹红岩 陈耀强*
(四川大学化学学院催化材料研究所, 成都 610064)

摘要: 制备了 Fe, Co, Cu, Cr 和 Mn 金属氧化物催化剂, 所用载体为 Al_2O_3-$Ce_{0.5}Zr_{0.5}O_2$ 复合氧化物. 利用 X 射线衍射(XRD), 程序升温还原(TPR), 储氧量测试, BET 比表面测试和光电子能谱(XPS)表征了催化剂. 并利用活性测试表征了各种催化剂对乙酸乙酯催化燃烧能力. 各种表征结果证实, 由于催化剂 Mn/Al_2O_3-$Ce_{0.5}Zr_{0.5}O_2$ (1:2, 质量比)具有最多的可还原物种, Cu/Al_2O_3-$Ce_{0.5}Zr_{0.5}O_2$ (1:2)具有较多的可还原物种和最强的可还原能力, 使它们对乙酸乙酯催化燃烧表现出了最好的活性. 在催化剂 Cu/Al_2O_3-$Ce_{0.5}Zr_{0.5}O_2$ (1:2)和 Mn/Al_2O_3-$Ce_{0.5}Zr_{0.5}O_2$ (1:2)上, 乙酸乙酯于 245 ℃转化了 99%, 表明这两种催化剂具有广泛的应用潜力.

关键词: 乙酸乙酯; 催化燃烧; 挥发性有机化合物
中图分类号: O643

Catalytic Combustion of Ethyl Acetate over Al_2O_3-$Ce_{0.5}Zr_{0.5}O_2$ Supported Metal Oxide Catalysts

YUAN Shu-Hua SHEN Mei GONG Mao-Chu WANG Jian-Li
YAN Sheng-Hui CAO Hong-Yan CHEN Yao-Qiang*
(*Institute of Catalytic Material Science, College of Chemistry, Sichuan University, Chengdu 610064, P. R. China*)

Abstract: The catalysts for the combustion of ethyl acetate were prepared using Fe, Co, Cu, Cr, and Mn metal oxides as active components supported on Al_2O_3-$Ce_{0.5}Zr_{0.5}O_2$ mixed oxides and characterized by X-ray diffraction (XRD), temperature programmed reduction (TPR), oxygen storage capacity measurement, BET surface area, XPS measurement, and activity test. According to the results of characterization, it was found that Cu/Al_2O_3-$Ce_{0.5}Zr_{0.5}O_2$ (1:2, mass ratio) and Mn/Al_2O_3-$Ce_{0.5}Zr_{0.5}O_2$ (1:2) catalysts presented excellent activity for the catalytic combustion of ethyl acetate, because of the more reducible species and high reducibility of the catalysts. For ethyl acetate oxidation, more than 99% conversion was achieved at 245 ℃ over catalysts Cu/Al_2O_3-$Ce_{0.5}Zr_{0.5}O_2$ (1:2) and Mn/Al_2O_3-$Ce_{0.5}Zr_{0.5}O_2$ (1:2, mass ratio), indicating that the catalysts had great potential for wide use.

Key Words: Ethyl acetate; Catalytic combustion; Volatile organic compound

Volatile organic compounds (VOCs) emitted from industrial processes and transportation activities, are recognized as major contributors to air pollution, either directly through their toxic and malodorous nature, or indirectly as ozone precursors and smog precursors[1]. By now, thermal incineration and catalytic oxidations have been used to remove VOCs. Thermal incineration is the most extended method to remove VOCs from industrial emissions, but this method requires rather high temperature, usually above 1000 ℃, and generates noxious byproducts (NO_x)[2]. Catalytic combustion is a more attractive alternative, since VOC oxidation over a catalyst takes place at temperatures much lower than those required for thermal destruction[3−6], and avoids the formation of nitrogen oxides.

The commercial catalysts used for VOCs removal from industrial emissions can be classified into three categories, supported noble metals (mainly Pt and Pd), metal oxides (supported or not),

Received: September 25, 2007; Revised: November 27, 2007; Published on Web: January 15, 2008.
English edition available online at www.sciencedirect.com
*Corresponding author. Email: nic7501@email.scu.edu.cn; Tel/Fax: +8628-85418451.
国家重点基础研究发展规划项目(973) (G1999022407)和国家高技术研究发展计划(863 项目)(2006AA06Z347)资助

mixtures of noble metals and metal oxides[7,8]. The supported noble metal catalysts are broadly used for VOCs combustion for their higher activity, but they are very easily poisoned and have higher cost than metal oxide catalysts. Thus, the development of metal oxide catalysts that have similar activity to the noble metal catalysts is crucial. At present, metal oxides are main transition metal oxides, such as oxides of chromium, cobalt, copper, nickel, and manganese[2,8,9].

In this study, the combustion of ethyl acetate (EAc) was studied, since EAc was found to be the most difficult to oxidize compound, and the activity of a catalyst for ethyl acetate oxidation would determine the catalytic behavior for oxidation of mixtures including ethyl acetate[8].

Amongst the transition metal oxides, manganese oxides are reported to be very active in the combustion of VOCs[10]. Ceria-zirconia mixed oxides as oxygen storage material can take up oxygen under oxidizing conditions and release it under reducing ones. Amongst ceria-zirconia mixed oxides catalysts, $Ce_{0.5}Zr_{0.5}O_2$ showed the best activity toward the oxidation of VOCs[11]. Accordingly, due to higher surface area of alumina, the catalytic combustion of ethyl acetate on Mn/Al_2O_3-$Ce_{0.5}Zr_{0.5}O_2$ mixed oxide catalysts with different mass ratios of Al_2O_3 to $Ce_{0.5}Zr_{0.5}O_2$ was first investigated to obtain the best combination of support. Then the Fe, Co, Cu, Cr, and Mn metal oxides were supported on the support and the catalyst behaviors were investigated. Monolithic catalysts have many advantages compared to particle catalysts, such as low pressure drop, high surface to volume ratio, thus in this study, the catalysts were washcoated on ceramic monoliths.

1 Experimental

1.1 Catalyst preparation

An alumina-supported manganese oxide material was prepared by impregnating of alumina with an aqueous solution of $Mn(NO_3)_2 \cdot 4H_2O$ (reagent grade) in excess of solution. Alumina support (10 g) was impregnated with 10 mL salt solution, and the excess water was removed in a water bath at 95 ℃. The catalyst was dried at 110 ℃ overnight and then calcined in static air at 500 ℃ for 2.5 h. This material was noted as Mn/Al_2O_3 and the manganese loading amount was 10% (mass fraction (w), dry basis). $Ce_{0.5}Zr_{0.5}O_2$ was synthesized using co-precipitation route from nitrate precursors and stabilized by calcinations in air at 600 ℃ for 4 h. $Ce_{0.5}Zr_{0.5}O_2$-supported manganese oxide material was also prepared by impregnating of $Ce_{0.5}Zr_{0.5}O_2$ with an aqueous solution of $Mn(NO_3)_2 \cdot 4H_2O$ (reagent grade) in excess of solution following the same route as the above procedure. This material was denoted as $Mn/Ce_{0.5}Zr_{0.5}O_2$. The catalysts were prepared by mixing $Mn/Ce_{0.5}Zr_{0.5}O_2$ material and Mn/Al_2O_3 material, with the mass ratio of $Mn/Ce_{0.5}Zr_{0.5}O_2$ to Mn/Al_2O_3 changing from 1:2 to 1:1, 2:1. These catalysts were denoted as Mn/Al_2O_3-$Ce_{05}Zr_{05}O_2$ (2:1), Mn/Al_2O_3-$Ce_{05}Zr_{05}O_2$ (1:1), Mn/Al_2O_3-$Ce_{0.5}Zr_{0.5}O_2$ (1:2), respectively.

Then all the catalysts prepared were washcoated on ceramic honeycomb. And the coating amount was kept at 180 $g \cdot L^{-1}$ during the experiment. The slurry solution was made by mixing the catalyst powder with appropriate amount of water. The honeycomb was first dipped in the slurry solution and then dried at 110 ℃ overnight and calcined at 500 ℃ for 2.5 h in static air.

Fe, Co, Cu, and Cr metal oxide catalysts were prepared following the same procedure as the preparation of Mn/Al_2O_3-$Ce_{0.5}Zr_{0.5}O_2$(1:2), using the nitrate solution of Fe, Co, Cu, Cr to impregnate Al_2O_3 and $Ce_{0.5}Zr_{0.5}O_2$.

1.2 Catalysts characterization

X-ray diffraction (XRD) studies were carried out on a DX-1000 X-ray diffractometer using Cu K_α (λ=0.15406 nm) radiation equipped with a graphite monochromator. The X-ray tube was operated at 45 kV and 25 mA. Samples were scanned from 2θ of 10° up to 90° and the X-ray diffraction line positions were determined with a step size of 0.03° and a slit of 1°.

The temperature programmed reduction (TPR) experiments were carried out in a conventional flow apparatus equipped with a TCD. All the samples (0.05 g) were pre-treated in a quartz U-tube in an He stream (5% O_2/He) at 450 ℃ for 1 h, and then cooled to room temperature. Next, a gas stream of hydrogen (5% H_2/N_2) was flowed at a rate of 45 $mL \cdot min^{-1}$ (STP) through the sample. The temperature was raised from room temperature to 1100 ℃ (at a heating rate of 10 $℃ \cdot min^{-1}$), and the amount of consumed hydrogen was determined by a thermal conductivity detector (TCD) as a function of temperature.

The textural properties were determined by N_2 adsorption-desorption at −196 ℃ using ZXF-06 automotive adsorption apparatus (Northwest Research Institute of Chemical Industry). The samples were previously evacuated at 300 ℃ under high vacuum. Oxygen storage capacity was determined by measuring oxygen storage capacity in a conventional flow apparatus using TCD detector. All the samples (0.2 g) were pre-treated in a quartz U-tube in H_2 stream at 550 ℃ for 45 min, and then cooled to 200 ℃ under pure N_2 stream. Then a gas stream of oxygen was pulsed at a rate of 20 $mL \cdot min^{-1}$ through the sample.

XPS measurements were performed on XSAM800 using Al K_α X-ray source at 12 kV and 12 mA.

1.3 Experimental apparatus

Rota meters were used for accurate and stable control of gas flow rate. The reactor system comprises of a vertical tubular furnace of 30 cm length controlled by a PID controller. The reactor itself is quartz tube of 10.7 mm o.d., at the middle of which the honeycomb modules are placed. A K-type thermocouple is positioned into the catalyst bed for accurate measurement of catalyst temperature. All gas lines of the apparatus are kept at 120 ℃ to minimize VOC adsorption on the walls. The stream of ethyl acetate was generated by bubbling a flow of air through a saturator that was fixed at a certain temperature. Another gas stream was used to produce ethyl acetate with low concentration. An online gas chromatography (GC) device equipped with a GDX-101 column and FID detector was used for instant analysis of the ethyl acetate concentration in the reactant or product gas.

2 Results and discussion

2.1 Influence of support on the catalytic oxidation of ethyl acetate

Figs.1 and 2 present the activity results of different catalysts for ethyl acetate under the conditions of 3.7182% ethyl acetate in air, total flow of 200 mL·min^{-1} and 1.5636% ethyl acetate in air, total flow of 400 mL·min^{-1}, respectively. Based on the results of activity, it can be concluded that, the same catalyst exhibits different catalytic abilities for ethyl acetate under different reaction conditions. The complete conversion temperature of ethyl acetate over every kind of catalyst lowers with the decrease of reactant concentration although the total flow rate is increased. According to the conversion ratios of ethyl acetate over all catalysts at different temperatures, it can be seen that, catalyst Mn/Al_2O_3 exhibits the worst activity in higher temperature range and $Mn/Ce_{0.5}Zr_{0.5}O_2$ exhibits the worst activity in lower temperature range. Catalysts using Al_2O_3-$Ce_{0.5}Zr_{0.5}O_2$ (1:2) as supports all exhibit better activity in the range of experimental temperature; amongst them, catalyst Mn/Al_2O_3-$Ce_{0.5}Zr_{0.5}O_2$ (1:2) shows the best activity for ethyl acetate under two kinds of conditions, the conversion of ethyl acetate on catalyst Mn/Al_2O_3-$Ce_{0.5}Zr_{0.5}O_2$ (1:2) reaches 98.72% at 250 ℃ under the condition of 3.7182% ethyl acetate in air, total flow of 200 mL·min^{-1} and more than 99% at 200 ℃ under condition of 1.5636% ethyl acetate in air, total flow of 400 mL·min^{-1}. The activity results indicate that catalyst Mn/Al_2O_3-$Ce_{0.5}Zr_{0.5}O_2$ (1:2) gives the best combination of the support. Thus, this support is used in further study.

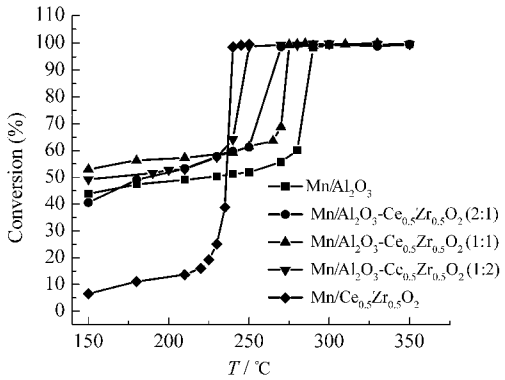

Fig.1 Conversions of ethyl acetate on different catalysts

3.7182% ethyl acetate in air, total flow: 200 mL·min^{-1}

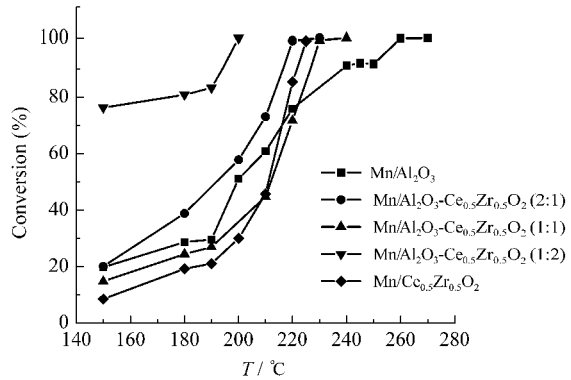

Fig.2 Conversions of ethyl acetate on different catalysts

1.5636% ethyl acetate in air, total flow: 400 mL·min^{-1}

Table 1 Textural properties and oxygen storage capacity of the catalysts

Catalyst	BET area ($m^2 \cdot g^{-1}$)	Pore volume ($mL \cdot g^{-1}$)	Mean pore diameter (nm)	Oxygen storage amount ($\mu mol \cdot g^{-1}$)
Co/Al_2O_3–$Ce_{0.5}Zr_{0.5}O_2$ (1:2)	57.75	0.13	60.15	1000.7
Mn/Al_2O_3–$Ce_{0.5}Zr_{0.5}O_2$ (1:2)	74.10	0.16	41.93	685.23
Cu/Al_2O_3–$Ce_{0.5}Zr_{0.5}O_2$ (1:2)	78.79	0.18	44.98	582.50
Fe/Al_2O_3–$Ce_{0.5}Zr_{0.5}O_2$ (1:2)	81.19	0.18	38.79	963.70
Cr/Al_2O_3–$Ce_{0.5}Zr_{0.5}O_2$ (1:2)	85.22	0.19	43.01	506.10

2.2 BET surface areas and oxygen storage capacity of prepared catalysts

The results of textural properties and oxygen storage capacity of the prepared catalysts are given in Table 1. From Table 1, it can be seen that both the BET surface area and pore volume increase following the sequence: Co, Mn, Cu, Fe, Cr. While oxygen storage capacity increases following another different sequence: Cr, Cu, Mn, Fe, Co. Catalysts Mn/Al_2O_3-$Ce_{0.5}Zr_{0.5}O_2$ (1:2) and Cu/Al_2O_3-$Ce_{0.5}Zr_{0.5}O_2$ (1:2) have mediate BET areas, pore volumes, and oxygen storage capacities. The results indicate that catalysts with the same support and different active components have quite different textural properties and oxygen storage capacities.

2.3 Crystalline phase analysis of prepared catalysts

The diffraction patterns of prepared catalysts are shown in Fig.3. The single CeO_2 fluorite structure phase is observed and quite weak γ-Al_2O_3 diffraction pattern is detected at 2θ=68° in all XRD patterns. Reflexes of CeO_2 fluorite structure are much stronger than those of γ-Al_2O_3, resulting in only quite weak γ-Al_2O_3 diffraction pattern because of overlay of reflexes of CeO_2 fluorite. Furthermore, only weak Co and Cu reflexes are observed over catalysts Co/Al_2O_3-$Ce_{0.5}Zr_{0.5}O_2$ (1:2) and Cu/Al_2O_3-$Ce_{05}Zr_{05}O_2$ (1:2), indicating that a little amount of metal happens to aggregate, and no Mn, Fe, Cr reflexes are observed on catalysts Mn/Al_2O_3-$Ce_{0.5}Zr_{0.5}O_2$ (1:2), Fe/Al_2O_3-$Ce_{0.5}Zr_{0.5}O_2$ (1:2) or Cr/Al_2O_3-$Ce_{0.5}Zr_{0.5}O_2$ (1:2), respectively, indicating that these metals are well dispersed on the surface of supports.

2.4 Redox properties

To investigate the reducibility of the catalysts with different active components, H_2 temperature programmed reduction (TPR) was used. As shown in Fig.4, catalyst Mn/Al_2O_3-$Ce_{0.5}Zr_{0.5}O_2$

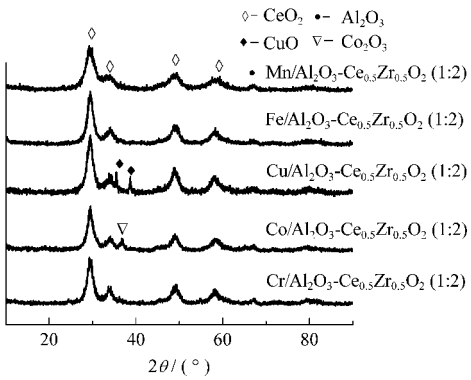

Fig.3 X-ray diffraction patterns of the catalysts

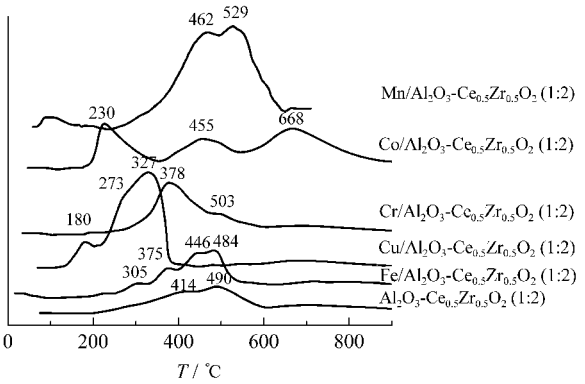

Fig.4 TPR profiles of the catalysts

(1∶2) shows the largest peak area of reduction and a two-step reduction process: the first peak at around 462 ℃ corresponds to the reduction of Mn^{4+} and Mn^{3+} ions to form the Mn_3O_4 spinel according to the reduction reactions, $MnO_2 \rightarrow Mn_2O_3 \rightarrow Mn_3O_4$; the second peak at around 529 ℃ is attributed to the reduction of Mn_3O_4 phase to MnO[12–15]. Moreover, the two peaks simultaneously also resulted from the reduction of the Ce^{4+} for the CeO_2-ZrO_2 solid solution.

Catalyst Co/Al_2O_3-$Ce_{0.5}Zr_{0.5}O_2$ (1∶2) exhibits three reduction peaks. The peaks can be attributed to the step-wise reduction of cobalt oxide *via* $Co_3O_4 \rightarrow CO_2O_3 \rightarrow CoO \rightarrow Co^0$. However, the peak at 455 ℃ may also be the reduction peak of the Ce^{4+} for the CeO_2-ZrO_2 solid solution, in this case, TPR spectrum of Co_3O_4 results in two peaks. This is in agreement with the results reported by Paryjczak[16], Brown[17], and Kang[18] *et al*..

Catalyst Cr/Al_2O_3-$Ce_{05}Zr_{05}O_2$ (1∶2) exhibits two reduction peaks with the first peak at 378 ℃ corresponding to the reduction of Cr_2O_3 and the second peak at 503 ℃ corresponding to the reduction of $Ce_{0.5}Zr_{0.5}O_2$. The reduction of Cr_2O_3 follows the course: $Cr_2O_3 \rightarrow CrO \rightarrow Cr^0$, as the intermediate CrO is very unstable, there is only one peak for Cr_2O_3 reduction. In the TPR profile of catalyst Cu/Al_2O_3-$Ce_{05}Zr_{05}O_2$ (1∶2), two main peaks at 180 and 327 ℃ with a shoulder at 273 ℃ are observed. According to the reports[19–21], the reactions involve in the copper-containing catalysts proceeds in the following mechanism:

$$CuO+H_2 \rightarrow Cu^0+H_2O \quad (1)$$

$$Cu^{2+}+0.5H_2 \rightarrow Cu^{+}+H^{+} \quad (2)$$

$$Cu^{+}+0.5H_2 \rightarrow Cu^0+H^{+} \quad (3)$$

Reactions (1) and (2) occur at a lower temperature than reaction (3)[22]. Thus, the first peak at 180 ℃ is ascribed to the reduction of CuO to metal Cu^0, and the shoulder at 273 ℃ is assigned to that of Cu^{2+} to Cu^+, while the peak at 327 ℃ is the signal of reduction of Cu^+ species to metal Cu^0. This is also in accordance with the result reported by Zhou *et al*.[23] and the peak at 327 ℃ is also attributed to the reduction of Ce^{4+} for the CeO_2-ZrO_2 solid solution, indicating that introduction of Cu lowers the reduction temperature of the Ce^{4+} for the CeO_2-ZrO_2 solid solution and greatly improves the reducible ability of the catalyst.

Catalyst Fe/Al_2O_3-$Ce_{05}Zr_{05}O_2$ (1∶2) exhibits four reduction peaks with maximum signals at 305, 375, 446, and 484 ℃, respectively. The last peak centered at 484 ℃ is attributed to the reduction of the Ce^{4+} for the CeO_2-ZrO_2 solid solution. From the other three reduction peaks, the existing form of the active component may be proposed. According to the published reports[24,25,17], the reduction of unsupported or supported Fe_2O_3 to metal Fe^0 occurs in three steps below 630 ℃, with Fe_3O_4 and FeO as the intermediates. Therefore, the three peaks can be assigned to the reduction of Fe_2O_3 to metal Fe^0. Thus, the element iron exists as Fe_2O_3 in the catalyst. As when blank experiment is carried out using the alumina support alone, no H_2-consumption peak is identified, the H_2-consumption peaks in Al_2O_3-$Ce_{0.5}Zr_{0.5}O_2$ (1∶2) are attributed to the reduction of $Ce_{0.5}Zr_{0.5}O_2$. The TPR profile of Al_2O_3-$Ce_{0.5}Zr_{0.5}O_2$ (1∶2) shows a two-peak pattern, the first low temperature signal located at 414 ℃ is assigned to the reduction of the surface, while the high temperature signal at 490 ℃ was assigned to the reduction of the bulk. The TPR profile of $Ce_{0.5}Zr_{0.5}O_2$, which is not shown here, also, shows a two-peak pattern with the temperature signal located at 449 and 585 ℃. This indicates that the adding of Al_2O_3 to $Ce_{0.5}Zr_{0.5}O_2$ greatly improves the reducibility of $Ce_{0.5}Zr_{0.5}O_2$ and interaction between Al_2O_3 and $Ce_{0.5}Zr_{0.5}O_2$. Based on the above analysis, it can be concluded that catalyst Cu/Al_2O_3-$Ce_{05}Zr_{05}O_2$ (1∶2) shows the lowest reduction temperature, indicat ing that it has the strongest reducibility; catalyst Mn/Al_2O_3-$Ce_{05}Zr_{05}O_2$ (1∶2) has the largest peak area of reduction, indicating that it possesses the most reducible species.

2.5 XPS analysis

The XPS spectra of active components Fe, Co, Cu, Cr, and Mn correspond to Fe 2*p*, Co 2*p*, Cu 2*p*, Cr 2*p*, and Mn 2*p*. The binding energies (E_B) of the elements listed in Table 2 indicate the presence of Fe_2O_3, Co_3O_4, CuO, Cr_2O_3, and MnO_2, respectively. This is in accordance with the results of TPR analysis. The XPS result of the catalyst Fe/Al_2O_3-$Ce_{05}Zr_{05}O_2$ (1∶2) further confirms the proposal that the existing form of iron in catalyst Fe/Al_2O_3-$Ce_{0.5}Zr_{0.5}O_2$ (1∶2) is Fe_2O_3.

Table 2 lists surface atom ratio (x) of each active component. Here, $x=[(A_i/Q_i)/(\Sigma A_i/Q_i)]\times 100\%$, A_i is the peak area of the active component while Q_i is the Q factor. From Table 2, it can be seen that on catalysts Cu/Al_2O_3-$Ce_{05}Zr_{05}O_2$ (1∶2), the active component Cu has the lowest surface concentration, indicating that more Cu enters the network structure of support or aggregates, which is well consistent with the appearance of Cu reflexes in the XRD patterns; while Cr concentration on the surface of catalyst Cr/Al_2O_3-$Ce_{05}Zr_{05}O_2$ (1∶2) is the highest, indicating that the Cr well disperses on the surface of support, which is approved by the results of XRD. Based on the above analyses, it can be concluded

Table 2 Values of E_B of the elements and surface atom ratio (x) of each active component

Catalyst	E_B/eV	x (%)
Cu 2*p*	780.8	0.72
Mn 2*p*	642.7	1.2
Co 2*p*	933.9	1.5
Fe 2*p*	711.8	1.9
Cr 2*p*	578.6	3.1

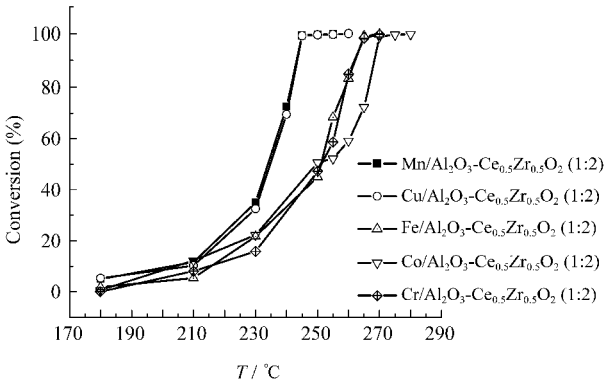

Fig.5 Conversion of ethyl acetate on different catalysts

2.4343% ethyl acetate in air, total flow: 400 mL·min^{-1}

that different active components supported on the same support exhibit different surface dispersive abilities, indicating that characteristics of active components themselves are responsible for different properties of corresponding catalysts.

2.6 Catalyst performance

Fig.5 shows the activity results of different catalysts for ethyl acetate (2.4343% in air). In the case of all the four catalysts, appreciable conversion of ethyl acetate is observed at 180 ℃. Catalysts Mn/Al_2O_3-$Ce_{0.5}Zr_{0.5}O_2$ (1∶2) and Cu/Al_2O_3-$Ce_{0.5}Zr_{0.5}O_2$ (1∶2) both exhibit the best activity for ethyl acetate, more than 99% conversion of ethyl acetate is achieved over these two kinds of catalysts at 245 ℃, while catalysts Co/Al_2O_3-$Ce_{0.5}Zr_{0.5}O_2$ (1∶2), Fe/Al_2O_3-$Ce_{0.5}Zr_{0.5}O_2$ (1∶2), and Cr/Al_2O_3-$Ce_{0.5}Zr_{0.5}O_2$ (1∶2) exhibit the worse activity for the catalytic oxidation of ethyl acetate, on which more than 99% conversion of ethyl acetate is achieved above 265 ℃. This can be presumably related to the difference interactions between ethyl acetate and catalytic surface. Furthermore, it is well known that the reduction process of cerium atom in cerium-zirconium mixed oxide occurrs according to the following equation:

$$Ce_xZr_{1-x}O_2+\delta H_2 \rightarrow Ce_xZr_{1-x}O_{2-\delta}+\delta H_2O+\delta V_O \quad (4)$$

Where the elimination of the capping oxygen anion as water molecules involves the appearance of an oxygen vacancy (V_O). The presence of those vacancies considerably promotes the mobility of oxygen from the bulk to the surface. Therefore, the amount of hydrogen consumption is proportional to the amount of oxygen vacancies, which is related to oxygen mobility. According to the above-mentioned results of TPR, catalyst Mn/Al_2O_3-$Ce_{0.5}Zr_{0.5}O_2$ (1∶2) has the largest reduction peak, indicating that it has the most oxygen vacancies and the oxygen mobility is more noticeably promoted for this catalyst; catalyst Cu/Al_2O_3-$Ce_{0.5}Zr_{0.5}O_2$ (1∶2) exhibits not only a larger peak area, but also the lowest reduction temperature, indicating that it shows more oxygen vacancies and the strongest oxygen mobility. Based on the above analyses, it can be concluded that the amount and ability of reduction species of catalysts are significantly responsible for the activity of catalysts for ethyl acetate.

3 Conclusions

Based on the results of all kinds of characterizations, it can be concluded that, metals Cu and Mn have better activity for the catalytic oxidation of ethyl acetate. More than 99% conversion of ethyl acetate is achieved over these two kinds of catalysts at 245 ℃, indicating the two kinds of catalysts have great potential for wide application.

Catalyst Cu/Al_2O_3-$Ce_{0.5}Zr_{0.5}O_2$ (1∶2) has the strongest reducibility; Mn/Al_2O_3-$Ce_{0.5}Zr_{0.5}O_2$ (1∶2) has the most reducible species, which are mainly responsible for better activity of catalysts irrelative to a considerable enough BET surface area, enough large storage oxide capacity, and surface dispersive ability of catalysts.

References

1 Kim, S. C. *J. Hazard. Mater. B,* **2002, 91**: 285
2 Álvarez-Galván, M. C.; de la Peña O′Shea, V. A.; Fierro, J. L. G.; Arias, P. L. *Catal. Commun.,* **2003, 4**: 223
3 Li, W. B.; Chu, W. B.; Zhuang, A.; Hua, J. *Catal. Today,* **2004, 93–95**: 205
4 Ihm, S. K.; Jun, Y. D.; Kim, D. C.; Jeong, K. E. *Catal. Today,* **2004, 93–95**: 149
5 van der Vaart, D. R.; Vatvuk, W. M.; Wele, A. H. *J. Air Waste Manage. Assoc.,* **1991, 41**: 92
6 Allen, C. C.; Blaney, B. L. *J. Air Pollut. Control Assoc.,* **1985, 35**: 841
7 Spivey, J. *J. Ind. Eng. Chem. Res.,* **1987, 26**: 2165
8 Papaefthimiou, P.; Ioannides, T.; Verykios, X. E. *Appl. Catal. B,* **1997, 13**: 175
9 Gandia, L. M.; Vicente, M. A.; Gil, A. *Appl. Catal. B,* **2002, 38**: 295
10 Baldi, M.; Finocchio, E.; Milella, F.; Busca, G. *Appl. Catal. B,* **1998, 16**: 43
11 Hinz, A.; Skoglundh, M.; Fridell, E.; Andersson, A. *J. Catal.,* **2001, 201**: 247
12 Sawyer, J. E.; Abraham, M. A. *Ind. Eng. Chem. Res.,* **1994, 33**: 2084
13 Hermia, J.; Vigneron, S. *Catal. Today,* **1993, 17**: 349
14 Gutiérrez-Ortiz, J. I.; de Rivas, B.; López-Fonseca, R.; González-Velasco, J. R. *Appl. Catal. A,* **2004, 269**: 147
15 Luo, M. F.; Yuan, X. X.; Zheng, X. M. *Appl. Catal. A,* **1998, 175**: 121
16 Paryjczak, T.; Rynkowski, J.; Karski, S. *J. Chromatogr. A,* **1980, 188**: 254
17 Brown, R.; Cooper, M. E.; Whan, D. A. *Appl. Catal. A,* **1982, 3**: 177
18 Kang, M.; Song, M. W.; Lee, C. H. *Appl. Catal. A,* **2003, 251**: 143
19 Sárkány, J.; d′Itri, J. L.; Sachtler, W. M. H. *Catal. Lett.,* **1992, 16**: 241
20 Jacobs, P. A.; Tielen, M.; Linart, J.; Uytterhoeven, J. B.; Beyer, H. *J. Chem. Soc., Faraday Trans. 1,* **1976, 72**: 2793
21 Gentry, S. J.; Hurst, N. W.; Jones, A. *J. Chem. Soc., Faraday Trans. 1,* **1979, 75**: 1688
22 Campa, M. C.; Indovina, V.; Minelli, G.; Moretti, G.; Pettiti, I.; Porta, P.; Riccio, A. *Catal. Lett.,* **1993, 23**: 141
23 Zhou, J.; Xia, Q. H.; Shen, S. C.; Kawi, S.; Hidajat. K. *J. Catal.,* **2004, 225**: 128
24 Unmuth, E. E.; Schwartz, L. H.; Butt, J. B. *J. Catal.,* **1980, 63**: 404
25 Wimmers, O. J.; Arnoldy, P.; Moulijn, J. A. *J. Phys. Chem.,* **1986, 90**: 1331